SCHOOL OF ENGINEERING
OLD DOMINION UNIVERSITY
NORFOLK, VIRGINIA

Technical Report 76T-16

DEVELOPMENT OF AN EFFICIENT NUMERICAL SCHEME FOR THE COMPUTATION OF TURBULENT BOUNDARY LAYER FLOWS OVER TWO-DIMENSIONAL AND AXISYMMETRIC BODIES

By

Veer N. Vatsa

and

G. L. Goglia

Progress Report

Prepared for the
National Aeronautics and Space Administration
Langley Research Center
Hampton, Virginia 23665

Under
Grant NSG 1226
September 2, 1975 - September 1, 1976
Dr. Julius E. Harris, Technical Monitor
High Speed Aerodynamics Division

Submitted by the
Old Dominion University Research Foundation
Norfolk, Virginia 23508

October 1976

TABLE OF CONTENTS

	Page
LIST OF TABLES	i
LIST OF FIGURES	i
LIST OF SYMBOLS	iii
INTRODUCTION	1
GOVERNING EQUATIONS	2
NUMERICAL ANALYSIS	7
VARIABLE GRID SCHEME	15
RESULTS AND DISCUSSION	18
CONCLUSIONS AND RECOMMENDATIONS	26
REFERENCES	39

LIST OF TABLES

Table 1.	Effect of iteration of wall shear.	27
Table 2.	Geometric progression constant employed by various investigators.	28

LIST OF FIGURES

Figure 1.	Effect of No. of intervals on step size at the wall.	29
Figure 2.	Geometric progression constant for $\overline{K} = 1.5$.	30
Figure 3.	Comparison of difference schemes.	31
Figure 4.	Effect of turbulence model.	32
Figure 5.	Turbulent flow over flat plate.	33
Figure 6.	Turbulent flow over sharp cone.	34
Figure 7A.	Heat transfer for sharp laminar cone with mass injection.	35
Figure 7B.	Velocity profile for sharp laminar cone with mass injection; X/L = 1.574.	36

LIST OF FIGURES (Concluded)

		Page
Figure 8A.	Heat transfer for spherical cap.	37
Figure 8B.	Wall shear for spherical cap.	38

LIST OF SYMBOLS

A	Damping function, $26\nu/u_\tau$
Al_n , Bl_n , Cl_n , Dl_n , El_n , Hl_n , Gl_n	Coefficients of difference form of momentum equation
$A2_n$, $B2_n$, $C2_n$, $D2_n$, $E2_n$, $H2_n$, $G2_n$	Coefficients of difference form of energy equation
C_p	Specific heat
D	Damping coefficient defined by equation (8)
$\tilde{F}$	Mass injection parameter defined by equation (65)
F	Normalized longitudinal velocity, u/u_e
j	$j = 0$ for 2 - D and $j = 1$ for axisymmetric flow
K	Geometric progression constant
K_1 , . . . K_n	Constants in eddy viscosity model
$\bar{K}$	Modified geometric progression constant defined by equation (51)
ℓ	Viscosity function defined by equation (23)
M	Mach number
N	Coordinate maping the η-coordinate, equation (47)
N_{p_r}	Prandtl number
NST	Nusselt number
p	Pressure
r	radius of curvature

r_0	Radius of curvature of the body surface
r_n	Nose radius for blunt body
R	Gas constant
S	Sutherland's constant
t	Transverse curvature parameter, r/r_0
T	Temperature
u	longitudinal velocity
$\tilde{v}$	Mean value of normal velocity
v	Transformed normal velocity
x , y	Body coordinates
X_1 , X_2 , X_3	Functions of longitudinal step size defined by equation (42)
$Y1_n$, . . . $Y6_n$	Functions of normal step size defined by equation (42)
α	Defined in equation (23)
β	Pressure gradient parameter defined by equation (23)
γ	Ratio of specific heats, C_p/C_v
$\overline{\gamma}$	Normal intermittency function
Γ	Longitudinal intermittency function
δ^*	Incompressible displacement thickness
Δ	Incremental value
ε	Eddy viscosity defined by equations (6-7)
$\overline{\varepsilon}$, $\tilde{\varepsilon}$	Eddy viscosity parameters defined by equations (4-5)
η	Normal coordinate in Levy-Lees transformation
Θ	Normalized temperature, T/T_e

μ	Viscosity
ν	Kinematic viscosity
ζ	Longitudinal coordinate in Levy-Lees transformation
ρ	Density
ϕ	Slope of body surface

Subscripts

e	Edge values
i	Inner layer
o	Outer layer
r	Reference value
t	Total or stagnation value
w	Wall value
max	Maximum value
∞	Free stream value

DEVELOPMENT OF AN EFFICIENT NUMERICAL SCHEME FOR THE COMPUTATION OF TURBULENT BOUNDARY LAYER FLOWS OVER TWO-DIMENSIONAL AND AXISYMMETRIC BODIES

by

Veer N. Vatsa[1] and G. Goglia[2]

INTRODUCTION

In view of the Stanford Conference (ref. 1) on turbulent flows, there is no apparent shortage of numerical methods for solving the equations governing the two-dimensional turbulent boundary layer flows. However, most existing methods require a large number of mesh points normal to the wall boundary in order to achieve good accuracy. The situation is still more alarming in three-dimensional flows where the computational effort is increased by an order of magnitude due to the added dimension and larger growth of boundary layer. Since the main objective is to develop efficient codes for three-dimensional flows, it is considered worthwhile to review the potential candidates from the existing methods for two-dimensional flows and either develop or select a scheme that is most efficient and suitable for future three-dimensional problems.

The two most promising schemes in the literature at the present time appear to be the Cebeci-Keller box scheme (ref. 2) and the Blottner variable grid scheme (ref. 3). The Keller box scheme has been shown to be very efficient for two-dimensional flows (ref. 2); however, it results in block-tridiagonal matrices and should require greater computational effort compared to simple tridiagonal matrices, especially for three-dimensional problems. Blottner has shown (ref. 3) that the variable grid scheme is equally good or better in comparison to the box scheme for two-dimensional flows, where he successfully employs large values of the geometric progression constant governing the normal mesh point distribution.

---

[1] Research Associate, Old Dominion University, Norfolk, Virginia 23508.

[2] Professor and Chairman, Department of Mechanical Engineering and Mechanics, Old Dominion University, Norfolk, Virginia 23508.

In view of the simplicity of the variable grid scheme, it was considered appropriate to conduct a study which would shed some light on the use of large values of the geometric progression constant and explain why the earlier attempts in this direction had failed. As a result of this study, a very efficient method has been developed. The concepts developed herein will be used in the three-dimensional research.

GOVERNING EQUATIONS

The governing equations used here are the classical boundary layer equations and can be found abundantly in literature (e.g., ref. 4); however, the particular form and transformations used here are similar to the ones presented by Van Driest (ref. 5) and used by Harris (ref. 6). For completeness, these are given below.

Continuity

$$\frac{\partial}{\partial x}\left(r^j \rho u\right) + \frac{\partial}{\partial y}\left(r^j \rho \tilde{v}\right) = 0 \tag{1}$$

Momentum

$$\rho\left[u\frac{\partial u}{\partial x} + \tilde{v}\frac{\partial u}{\partial y}\right] = -\frac{dp}{dx} + \frac{1}{r^j}\frac{\partial}{\partial y}\left(r^j \frac{\overline{\varepsilon}\partial u}{\partial y}\right) \tag{2}$$

Energy

$$\rho\left[u\frac{\partial}{\partial x}\left(C_p T\right) + \tilde{v}\frac{\partial}{\partial y}\left(C_p T\right)\right] = u\frac{dp}{dx} + \overline{\varepsilon}\left(\frac{\partial u}{\partial y}\right)^2 + \frac{1}{r^j}\frac{\partial}{\partial y}\left[r^j \tilde{\varepsilon}\frac{\partial}{\partial y}\left(C_p T\right)\right] \tag{3}$$

The conventional overbar notation to represent the mean-flow quantities has been dropped for the sake of simplicity. The eddy viscosity parameters $\overline{\varepsilon}$ and $\tilde{\varepsilon}$ are defined as follows:

$$\overline{\varepsilon} = \mu\left(1 + \frac{\varepsilon}{\mu}\Gamma\right) \tag{4}$$

$$\tilde{\varepsilon} = \frac{\mu}{N_{p_r}} \left(1 + \frac{\varepsilon}{\mu} \frac{N_{p_r}}{N_{p_{r,t}}} \cdot \Gamma \right) \tag{5}$$

A two-layer Cebeci-Smith (ref. 7) turbulence model, as described by Harris (ref. 6) is employed to calculate the eddy viscosity.

For the inner layer,

$$\left(\frac{\varepsilon}{\mu}\right)_i = \frac{\rho}{\mu} (K_1 \, yD)^2 \left|\frac{\partial u}{\partial u}\right| , \quad (0 \leq y \leq y_m) \quad , \tag{6}$$

and for the outer region,

$$\left(\frac{\varepsilon}{\mu}\right)_o = \frac{\rho}{\mu} K_2 \, u_e \, \delta^*_{inc} \, \overline{\gamma} , \quad (y_m < y) \quad , \tag{7}$$

where y_m is the value of y where the curves for inner and outer eddy viscosity intersect each other. In the above expressions,

$$D = 1 - \exp \left\{ - \left[\sqrt{\frac{\nu w}{\nu}} (1 + K3) - K3 \right] \frac{y}{A} \right\} \tag{8}$$

is the damping coefficient,

$$\delta^*_{inc} = \int_o^\infty \left(1 - \frac{u}{u_e} \right) dy \tag{9}$$

is the incompressible displacement thickness, and

$$\overline{\gamma} = \frac{1 - \text{erf} \left[5 \left(\frac{y}{\delta} - K4 \right) \right]}{2} \tag{10}$$

is the normal intermittency distribution coefficient.

The boundary layer thickness δ is defined as the distance normal to the wall boundary where $u/u_e = 0.995$. The empirical constants k_1 , k_2 , k_3 , and k_4 are set equal to .4 , .0168 , 0.0 and .78 respectively. Location of y_m is determined from the continuity of eddy viscosity, so that

$$\left(\frac{\varepsilon}{\mu}\right)_i = \left(\frac{\varepsilon}{\mu}\right)_o \quad \text{at} \quad y = y_m \ . \tag{11}$$

The turbulent Prandtl number $N_{p_{r,t}}$ is assumed constant and is set equal to 0.95 .

Finally, there are two algebraic relations,

$$p = \rho RT \tag{12}$$

and the viscosity law, chosen here to be Sutherland's viscosity law,

$$\frac{\mu}{\mu_r} = \left(\frac{T}{T_r}\right)^{3/2} \left(\frac{T_r + S}{T + S}\right) \tag{13}$$

where the reference temperature is

$$T_r = \frac{u_\infty^2}{R}$$

and $S = 198.6^0$ R is the Sutherland's constant.

The above set of governing equations is transformed in terms of the Levy-Lees variables to

$$\zeta\ (x) = \int_o^x \rho_e\ \mu_e\ u_e\ {r_o}^{2j}\ dx \tag{15}$$

and

$$\eta\ (x,\ y) = \frac{\rho_e\ u_e\ {r_o}^j}{\sqrt{2\zeta}} \int_o^y t^j \left(\frac{\rho}{\rho_e}\right) dy \ , \tag{16}$$

where

$$t = \frac{r}{r_o} \tag{17}$$

is the transverse curvature term. Defining new dependent variables as

$$F = \frac{u}{u_e} , \quad \Theta = \frac{T}{T_e} \tag{18}$$

and a transformed normal velocity as

$$v = \frac{2\zeta}{\rho_e \, u_e \, \mu_e \, r_o^{2j}} \left[F \left(\frac{\partial \eta}{\partial x} \right) + \frac{\rho \, \tilde{v} \, r_o^{j} \, t^{j}}{\sqrt{2\zeta}} \right] , \tag{19}$$

the governing equations in the transformed variables then become

Continuity

$$\frac{\partial v}{\partial \eta} + 2\zeta \, \frac{\partial F}{2\zeta} + F = 0 , \tag{20}$$

Momentum

$$2\zeta \, F \, \frac{\partial F}{2\zeta} + v \, \frac{\partial F}{\partial \eta} - \frac{\partial}{\partial \eta} \left(t^{2j} \, \ell \, \bar{\varepsilon} \, \frac{\partial F}{\partial \eta} \right) + \beta \, (F^2 - \Theta) = 0 , \quad \text{and} \tag{21}$$

Energy

$$2\zeta \, F \, \frac{\partial \Theta}{\partial \zeta} + v \, \frac{\partial \Theta}{\partial \eta} - \frac{\partial}{\partial \eta} \left(t^{2j} \, \frac{\ell}{N_{p_r}} \, \tilde{\varepsilon} \, \frac{\partial \Theta}{\partial \eta} \right) - \alpha \, \ell \, t^{2j} \, \bar{\varepsilon} \left(\frac{\partial F}{\partial \eta} \right)^2 = 0 , \tag{22}$$

where

$$\alpha = \frac{u_e^{\,2}}{C_p \, T_e} , \quad \beta = \frac{2\zeta}{u_e} \left(\frac{due}{d\zeta} \right), \quad \text{and} \quad \ell = \frac{\rho \mu}{\rho_e \, \mu_e} . \tag{23}$$

The physical normal coordinate is related to the transformed variable through the relation

$$y = \frac{r_o}{\cos \phi} \left[- 1 \pm \left(\frac{1 + 2 \sqrt{2\zeta} \cos \phi}{\rho_e u_e r_o{}^2 j} \int_o^\eta \Theta \, d \eta \right)^{1/2} \right], \quad (24)$$

where the positive sign is taken for external flow and the negative sign is used for internal flow.

The boundary conditions at the wall are

$$\left.\begin{aligned} F (\zeta, 0) &= 0 \\ \Theta (\zeta, 0) &= \Theta_w (\zeta) \quad \text{or} \quad \left(\frac{\partial \Theta}{\partial \eta}\right)_{\zeta, 0} = \left(\frac{\partial \Theta}{\partial \eta}\right)_w \\ v (\zeta, 0) &= v_w (\zeta) \end{aligned}\right\} , \quad (25)$$

and the outer edge conditions are

$$\left.\begin{aligned} F (\zeta, \eta_e) &= 1 \\ \Theta (\zeta, \eta_e) &= 1 \end{aligned}\right\} . \quad (26)$$

Note that the transformed normal velocity in terms of physical variables is

$$v_w = \frac{\sqrt{2\zeta}}{\mu_e r_o{}^2 j} \left(\frac{\rho_w v_w}{\rho_e u_e} \right) . \quad (27)$$

Transition. The starting location and extent of the transition have to be supplied to the computer code. Such estimates are generally semi-empirical in nature, based on correlations obtained from existing data. With these two parameters fixed, the intermittency distribution is calculated using the equation

$$\Gamma (\bar{\zeta}) = 1 - \exp (- .412 \, \bar{\zeta}^2) \quad (28)$$

where

$$\bar{\zeta} = \frac{x - x_{t,i}}{(x)_{\Gamma=3/4} - (x)_{\Gamma=1/4}} \quad . \tag{29}$$

The reader is referred to the original work of Harris (refs. 6, 8) for the details of the intermittency distribution and turbulence model.

This completes the set of governing differential equations for laminar, transitional and turbulent flow past two-dimensional and axisymmetric bodies.

NUMERICAL ANALYSIS

Due to the steepness of the profiles near the wall, it is not practical to use an equally spaced mesh for the calculation of turbulent boundary layer flows. A practical solution to this problem is to use a mesh which has short steps near the wall boundary, but lengthens the step size away from the wall. A very effective way of achieving this objective is to select the mesh in the normal direction such that the successive mesh widths $\Delta\eta_i$ form a geometric progression according to the relation

$$\Delta\eta_i = (k)^{i-1} \Delta\eta_1 \ , \ (i = 1, 2, \ . \ . \ . \ n_{max}) \tag{30}$$

where k is the geometric progression constant.

Once the mesh distribution is defined, a choice must be made between the various difference schemes. The computer code used for the present study has an option of using either (a) the difference relations obtained by using three terms of the Taylor series expansion, so that the first truncated term is proportional to the third derivative for both first and second derivative expressions, or (b) the difference relations obtained by truncating the terms proportional to $\Delta\eta_i$, which is equivalent to using two terms for the first derivative and three terms for the second derivative from the Taylor series expansion. The first approach will be referred

to as the conventional differencing approach since it has been used by most authors in the field (refs. 6, 7, 9). The second approach will be called Blottner's differencing approach after Blottner (ref. 3). The resulting expressions along with the error terms are as follows:

A. Conventional difference expressions

$$\left.\frac{\partial u}{\partial \eta}\right|_n = \frac{\Delta\eta_{n-1}}{\Delta\eta_n}\quad\frac{u_{n+1}}{(\Delta\eta_{n-1}+\Delta\eta_n)} - \frac{(\Delta\eta_{n-1}-\Delta\eta_n)}{\Delta\eta_n-\Delta\eta_{n-1}}\,u_n$$

$$-\frac{\Delta\eta_n}{\Delta\eta_{n-1}}\quad\frac{u_{n-1}}{(\Delta\eta_{n-1}+\Delta\eta_n)} - \frac{\Delta\eta_{n-1}\,\Delta\eta_n}{6}\,\frac{\partial^3 u}{\partial\eta_3} \qquad (31)$$

and

$$\frac{\partial^2 u}{\partial\eta_2} = \frac{2u_{n+1}}{\Delta\eta_n\,(\Delta\eta_n+\Delta\eta_{n-1})} + \frac{2u_{n-1}}{\Delta\eta_{n-1}\,(\Delta\eta_n+\Delta\eta_{n-1})}$$

$$-\frac{2u_n}{\Delta\eta_{n-1}\,\Delta\eta_n} - \frac{(\Delta\eta_n-\Delta\eta_{n-1})}{3}\,\frac{\partial^3 u}{\partial\eta_3}\ . \qquad (31)$$

The nonlinear term is written as

$$\frac{\partial}{\partial\eta}\left(\ell\,\frac{\partial u}{\partial\eta}\right) = \ell\,\frac{\partial^2 u}{\partial\eta_2} + \frac{\partial\ell}{\partial\eta}\,\frac{\partial u}{\partial\eta} \qquad (33)$$

so that the first truncated term

$$= -\frac{(\Delta\eta_n-\Delta\eta_{n-1})}{12}\left[3\,\ell\,\frac{\partial^3 u}{\partial\eta_3} + 6\,\frac{\partial^2\ell}{\partial\eta_2}\,\frac{\partial u}{\partial\eta} + 6\,\frac{\partial^2 u}{\partial\eta_2}\,\frac{\partial\ell}{\partial\eta}\right]_n . \qquad (34)$$

B. Blottner's difference expressions

$$\frac{\partial u}{\partial\eta} = \frac{u_{n+1}-u_{n-1}}{(\Delta\eta_{n-1}+\Delta\eta_n)} - \frac{(\Delta\eta_n-\Delta\eta_{n-1})}{2}\,\frac{\partial^2 u}{\partial\eta_2}\ , \qquad (35)$$

and

$$\frac{\partial^2 u}{\partial \eta_2} = \frac{\partial}{\partial \eta}\left(\frac{\partial u}{\partial \eta}\right) = \frac{2u_{n+1}}{\Delta\eta_n\,(\Delta\eta_n + \Delta\eta_{n-1})} - \frac{2u_n}{\Delta\eta_{n-1}\,\Delta\eta_n}$$

$$+ \frac{2u_{n-1}}{\Delta\eta_{n-1}\,(\Delta\eta_n + \Delta\eta_{n-1})} - \frac{(\Delta\eta_n - \Delta\eta_{n-1})}{3}\frac{\partial^3 u}{\partial \eta_3} \quad , \qquad (36)$$

and the nonlinear term is written as

$$\frac{\partial}{\partial \eta}\left(\ell\,\frac{\partial u}{\partial \eta}\right) = \frac{2}{\Delta\eta_n + \Delta\eta_{n-1}}\left[\ell_{n+1_2}\left(\frac{u_{n+1} - u_n}{\Delta\eta_n}\right)\right.$$

$$\left. - \ell_{n-1_2}\left(\frac{u_n - u_{n-1}}{\Delta\eta_{n-1}}\right)\right] - \frac{1}{12}\left[\ell\,\frac{\partial^3 u}{\partial \eta_3} + 3\,\frac{\partial^2}{\partial \eta_2}\right.$$

$$\left.\cdot\left(\ell\,\frac{\partial u}{\partial \eta}\right)\right]_n (\Delta\eta_n - \Delta\eta_{n-1}) \quad . \qquad (37)$$

Replacing the derivatives with their difference approximations, the governing equations can be written as follows:

Momentum

$$Al_n\,F_{m+1,n-1} + Bl_n\,F_{m+1,n} + Cl_n\,F_{m+1,n+1} + Dl_n\,\Theta_{m+1,n-1}$$

$$+ El_n\,\Theta_{m+1,n} + Hl_n\,\Theta_{m+1,n+1} = Gl_n \quad , \qquad (38)$$

and

Energy

$$A2_n\,F_{m+1,n-1} + B2_n\,F_{m+1,n} + C2_n\,F_{m+1,n+1} + D2_n\,\Theta_{m+1,n-1}$$

$$+ E2_n\,\Theta_{m+1,n} + F2_n\,\Theta_{m+1,n+1} = G2_n \quad . \qquad (39)$$

The coefficients Al_n , Bl_n , . . . , $G2_n$ are functions of the known quantities at stations m and $m-1$ or of current values of quantities at station $m+1$. The specific form of these coefficients are

A. Conventional Approach

Momentum

$$Al_n = -\,(V_{m+1,n})_G \cdot Y6_n + \frac{\partial}{\partial\eta}\,(t^{2j}\,\ell\bar{\varepsilon})_{m+1,n} \cdot Y6_n - (t^{2j}\,\ell\bar{\varepsilon})_{m+1,n} \cdot Y3_n$$

$$Bl_n = \frac{\zeta\,(F_{m+1,n})_G}{\Delta\zeta 2} \cdot X1 - (V_{m+1,n})_G \cdot Y5_n + \frac{\partial}{\partial\eta}\,(t^{2j}\,\ell\bar{\varepsilon})_{m+1,n} \cdot Y5_n + (t^{2j}\,\ell\bar{\varepsilon})_{m+1,n} \cdot Y2_n + 2\beta\,(F_{m+1,n})_G$$

$$Cl_n = (V_{m+1,n})_G \cdot Y4_n - \frac{\partial}{\partial\eta}\,(t^{2j}\,\ell\bar{\varepsilon})_{m+1,n} \cdot Y4_n - (t^{2j}\,\ell\bar{\varepsilon})_{m+1,n} \cdot Y1_n$$

$$Dl_n = 0$$

$$El_n = -\,\beta_{m+1}$$

$$Hl_n = 0$$

$$Gl_n = \frac{\zeta\,(F_{m+1,n})_G}{\Delta\zeta 2}\,[(X2)\,F_{m,n} - (X3)\,F_{m-1,n}] + \beta\,(F_{m+1,n})_G^2 \,. \qquad (40)$$

Note that m is the running index in ζ-direction, m+1 being the the current station, and n is the running index in η-direction. The governing equations are being solved at (m+1,n) point.

Energy

$$A2_n = 2 \left(\frac{\partial F}{\partial \eta}\right)_{\substack{m+1,n \\ G}} \cdot (\alpha \ell t^{2j} \bar{\varepsilon})_{m+1,n} \cdot Y6_n$$

$$B2_n = 2 \left(\frac{\partial F}{\partial \eta}\right)_{\substack{m+1,n \\ G}} \cdot (\alpha \ell t^{2j} \bar{\varepsilon})_{m+1,n} \cdot Y5_n$$

$$C2_n = -2 \left(\frac{\partial F}{\partial \eta}\right)_{\substack{m+1,n \\ G}} \cdot (\alpha \ell t^{2j} \bar{\varepsilon})_{m+1,n} \cdot Y4_n$$

$$D2_n = -(v_{m+1,n})_G \cdot Y6_n + Y6_n \cdot \frac{\partial}{\partial \eta} (C\ell\tilde{\varepsilon})_{m+1,n} - Y3_n \cdot \left(\frac{C\ell\tilde{\varepsilon}}{\sigma}\right)_{m+1,n}$$

$$E2_n = \frac{\zeta (F_{m+1,n})_G}{\Delta\zeta 2} \cdot X1 - (v_{m+1,n})_G \cdot Y5_n + Y5_n \cdot \frac{\partial}{\partial \eta} (C\ell\bar{\varepsilon})_{m+1,n} + \left(\frac{C\ell\tilde{\varepsilon}}{\sigma}\right)_{m+1,n} \cdot Y2_n$$

$$H2_n = (v_{m+1,n})_G \cdot Y4_n - Y4_n \cdot \frac{\partial}{\partial \eta} (C\ell\bar{\varepsilon})_{m+1,n} - \left(\frac{C\ell\tilde{\varepsilon}}{\sigma}\right)_{m+1,n} \cdot Y1_n$$

$$G2_n = \frac{\zeta (F_{m+1,n})_G}{\Delta\zeta 2} [(X2)\ \Theta_{m,n} - (X3)\ \Theta_{m-1,n}] - (\alpha \ell t^{2j} \bar{\varepsilon})_{m+1,n} \left(\frac{\partial F}{\partial \eta}\right)^2_{\substack{m+1,n \\ G}} \qquad (41)$$

where

$$Y1_n = \frac{2}{\Delta\eta_n (\Delta\eta_n + \Delta\eta_{n-1})}$$

$$Y2_n = \frac{2}{\Delta\eta_n \, \Delta\eta_{n-1}}$$

$$Y3_n = \frac{-2}{\Delta\eta_{n-1} \, (\Delta\eta_n + \Delta\eta_{n-1})}$$

$$Y4_n = \frac{\Delta\eta_{n-1}}{\Delta\eta_n \, (\Delta\eta_n + \Delta\eta_{n-1})}$$

$$Y5_n = \frac{\Delta\eta_{n-1} - \Delta\eta_n}{\Delta\eta_n \, \Delta\eta_{n-1}}$$

$$Y6_n = \frac{\Delta\eta_n}{\Delta\eta_{n-1} \, (\Delta\eta_n + \Delta\eta_{n-1})}$$

$$X1 = 2 \, \frac{\Delta\zeta_1 + 2\Delta\zeta_2}{\Delta\zeta_1 + \Delta\zeta_2}$$

$$X2 = 2 \, \frac{\Delta\zeta_1 + \Delta\zeta_2}{\Delta\zeta_1}$$

$$X3 = 2 \, \frac{\Delta\zeta_1 \, \Delta\zeta_2}{\Delta\zeta_1 \, (\Delta\zeta_1 + \Delta\zeta_2)} \qquad (42)$$

B. Blottner's Approach

Momentum

$$A1_n = \frac{(v_{m+1,n})_G}{\Delta\eta_{n-1} + \Delta\eta_n} - \left[\frac{(t^{2j} \, \ell \, \bar{\varepsilon})_{m+1,n} + (t^{2j} \, \ell \, \bar{\varepsilon})_{m+1,n-1}}{2} \right] \cdot Y3_n$$

$$Bl_n = \frac{\zeta\ (F_{m+1,n})_G}{\Delta\zeta 2} \cdot Xl + \left[\frac{(t^{2j}\ \ell\ \bar{\varepsilon})_{m+1,n} + (t^{2j}\ \ell\ \bar{\varepsilon})_{m+1,n+1}}{2}\right] \cdot Yl_n + \left[\frac{(t^{2j}\ \ell\ \bar{\varepsilon})_{m+1,n} + (t^{2j}\ \ell\ \bar{\varepsilon})_{m+1,n-1}}{2}\right] \cdot Y3_n + 2\beta\ (F_{m+1,n})_G$$

$$Cl_n = \frac{(v_{m+1,n})_G}{\Delta\eta_{n-1} + \Delta\eta_n} - \left[\frac{(t^{2j}\ \ell\ \bar{\varepsilon})_{m+1,n} + (t^{2j}\ \ell\ \bar{\varepsilon})_{m+1,n+1}}{2}\right] \cdot Yl_n$$

$$Dl_n = 0$$

$$El_n = -\beta$$

$$Hl_n = 0$$

$$Gl_n = \frac{\zeta\ (F_{m+1,n})_G}{\Delta\zeta}\ [(X2)\ F_{m,n} - (X3)\ F_{m-1,n}] - \beta\ (F_{m+1,n})_G^2 \cdot \qquad (43)$$

Energy

$$A2_n = 2\ (\alpha\ \ell\ t^{2j}\ \dot{\bar{\varepsilon}})_{m+1,n} \cdot \left(\frac{\partial F}{\partial \eta}\right)_{\substack{m+1,n \\ G}} \Big/ (\Delta\eta_{n-1} + \Delta\eta_n)$$

$$B2_n = 0$$

$$C2_n = -2\ (\alpha\ \ell\ t^{2j}\ \bar{\varepsilon})_{m+1,n} \cdot \left(\frac{\partial F}{\partial \eta}\right)_{\substack{m+1,n \\ G}} \Big/ (\Delta\eta_{n-1} + \Delta\eta_n)$$

$$D2_n = -\frac{(v_{m+1,n})_G}{\Delta\eta_{n-1} + \Delta\eta_n} - .5\left[\left(t^{2j}\frac{\ell}{\sigma}\tilde{\varepsilon}\right)_{m+1,n} + \left(t^{2j}\frac{\ell}{\sigma}\tilde{\varepsilon}\right)_{m+1,n-1}\right] \cdot Y3_n$$

$$E2_n = \frac{\zeta\,(F_{m+1,n})}{\Delta\zeta 2} \cdot X1 + .5\left[\left(t^{2j}\frac{\ell}{\sigma}\tilde{\varepsilon}\right)_{m+1,n} + \left(t^{2j}\frac{\ell}{\sigma}\tilde{\varepsilon}\right)_{m+1,n-1}\right] \cdot Y1_n + .5\left[\left(t^{2j}\frac{\ell}{\sigma}\tilde{\varepsilon}\right)_{m+1,n} + \left(t^{2j}\frac{\ell}{\sigma}\tilde{\varepsilon}\right)_{m+1,n-1}\right] \cdot Y3_n$$

$$H2_n = \frac{(v_{m+1,n})_G}{\Delta\eta_{n-1} + \Delta\eta_n} - .5\left[\left(t^{2j}\frac{\ell}{\sigma}\tilde{\varepsilon}\right)_{m+1,n} + \left(t^{2j}\frac{\ell}{\sigma}\tilde{\varepsilon}\right)_{m+1,n+1}\right] \cdot Y1_n$$

$$G2_n = \frac{\zeta\,(F_{m+1,n})}{\Delta\zeta 2}\left[(X2)\,\Theta_{m,n} - (X3)\,\Theta_{m-1,n}\right] - (\alpha\,\ell\,t^{2j}\,\bar{\varepsilon})_{m+1,n} \cdot \left(\frac{\partial F}{\partial\eta}\right)^2_{\substack{m+1,n\\ G}} \cdot \qquad (44)$$

These equations are solved using the coupled solution technique of the type used by Harris (ref. 6) and described in detail by Price and Harris (ref. 10). Once the momentum and energy equations are solved, the continuity equation is integrated using the trapezoidal rule of integration, and then the eddy viscosity is updated. Due to the presence of nonlinearities in this set of equations, iteration is required to update the nonlinear coefficients. To study the effect of iteration, solutions were obtained for a flat plate at $M_\infty = 2.8$ and varying the maximum number of iterations allowed from 0 to 15. The results thus obtained with 25 points in the boundary layer are presented in table 1 and clearly indicate that it is sufficient to iterate only once to obtain accurate results. For this reason, all the calculations presented in this report are made by iterating only once. For more details of the numerical technique, the reader is referred to the original paper by Price and Harris (ref. 10).

It should be noted that the starting solution is obtained here by taking the self-similar form of the governing equations and integrating these by standard tridiagonal procedures developed for solving the parabolic equations (ref. 11), in contrast to the Runge-Kutta procedure of reference 10.

VARIABLE GRID SCHEME

It has previously been indicated that a variable grid which accomodates shorter steps near the wall boundary and longer steps away from it is the practical way to compute turbulent boundary layer flows. The most popular approach seems to be the use of a mesh such that the successive step widths form a geometric progression series (e.g., refs. 2, 3, 6 to 10). Thus, any two consecutive step widths have a fixed ratio k, known as the geometric progression constant. The value of k plays a significant role on the numerical accuracy. Some of the typical values of k and the number of points in the boundary layer employed by various authors are given in table 2, which shows the range of (ref. 12-17) k in use to be 1.02 to 1.12. Shang et al. (ref. 16) presented the error in wall shear versus k, and their results indicate that by using a value of $k = 1.12$, instead of 1.02, the computation time is reduced by a factor of 7.6. But for this large value of k ($k = 1.12$), there is an error of about seven percent in the wall shear. To achieve an accuracy of one percent, the scheme of reference 16 would require about 220 points and $k \approx 1.04$. Although such detailed error analysis is not available in the open literature, it seems to be the basic reason for avoiding the use of larger values of k. An exception to this conventional approach is a recent study by Blottner (ref. 3), where he used $k = 1.82$ and obtained satisfactory results with 10 to 20 points in the boundary layer. It should be mentioned that the k used by Blottner differs from the conventional definition of the geometric progression constant, and an attempt is made here to relate the two.

In the geometric progression, the nth step size is as follows:

$$\Delta\eta_n = \Delta\eta_1 \, k^{n-1} \tag{45}$$

where k is the conventional geometric progression constant. Consequently, the η-coordinate at the nth point is

$$\eta_n = \eta_{max} \left[\frac{k^{n-1} - 1}{k^{n_{max}-1} - 1} \right] . \tag{46}$$

Blottner interprets the variable grid as a coordinate transformation (ref. 3) where the nonuniformly varying η-coordinate (0 to η_{max}) is transformed point by point to a uniformly varying N-coordinate (0 to 1), the mapping being given by the relation of the type

$$\eta_n = \eta \ (N_n) \qquad (n = 1, 2, \ldots, n_{max}) , \tag{47}$$

where

$$N_n = (n - 1) \ \Delta N$$

and

$$N_{max} = 1 \ ; \tag{48}$$

therefore,

$$\eta_n = \eta_{max} \left[\frac{k^{Nn/\Delta N} - 1}{k^{1/\Delta N} - 1} \right] \tag{49}$$

It should be noted that this is not a very suitable definition of k for conducting a step size study. To clarify this point, consider a uniformly spaced grid. In a step size study, if the number of grid points are doubled, the denser mesh puts one point exactly in the middle of any two consecutive points of the coarser mesh in addition to the points that coincide with the original coarse mesh. Consequently, there is a linear relationship between the number of mesh points and the step size. Although an exact linear

relationship between the step size and the number of grid points is not possible in a variable grid, we can approximate such a condition near the wall boundary by imposing the following limiting condition:

$$k \to 1 \quad \text{as} \quad \Delta N \to 0 \quad . \tag{50}$$

This can be satisfied if a modified geometric progression constant $\bar{k}$ is defined as

$$\bar{k} = (k)^{\Delta N_o/\Delta N} \tag{51}$$

where ΔN_o is the step width in the uniformly varying coordinate-N, corresponding to N_o, the reference value chosen for number of grid points.

Thus, equation (49) takes the form

$$\eta_n = \eta_{max} \left[\frac{(\bar{k})^{N_n/\Delta N_o} - 1}{(\bar{k})^{1/\Delta N_o} - 1} \right] , \tag{52}$$

which is given as the starting relation for geometric progressions by Blottner (ref. 3).

With the modified definition of $\bar{k}$, a uniform spacing and, hence, a linear relationship between step size and the number of grid points is obtained in the y-coordinate for infinitely many points.

As a specific case, let $\eta_{max} = 77.7$ and $\bar{k} = 1.5$ for $N_o = 25$. The step size $\Delta\eta_1$ at the wall, obtained by using equation (52), is plotted versus the number of intervals on a log-log scale (fig. 1) and clearly indicates a linear trend for $N > 60$. The corresponding values of physical k are plotted as a function of the number of intervals in figure 2 for the sake of completeness. If a similar study was conducted with the conventional k, the slope of the curve in figure 1 would be much steeper.

It should be noted that such a modified definition of the geometric progression constant is fundamental to any step size study for a variable grid; otherwise, one gets into a situation similar to the one encountered by Shang et al. (ref. 16). In reference 16, the value of $\Delta\eta_1$ was fixed, and k was varied between 1.02 and 1.12. The results thus obtained showed a seven percent error in wall shear for $k = 1.12$ and $N = 86$, thereby eliminating the use of higher values of k. In contrast, it will be shown that with the variable grid scheme discussed here, reasonably accurate solutions are obtained with $k = 1.5$ and $N = 25$.

RESULTS AND DISCUSSION

The results of this study can be divided into two categories: the first part being concerned with the study and development of an efficient numerical procedure to minimize the required number of grid points normal to the wall boundary and the second part being concerned with the application of the selected scheme to various boundary layer flows.

Before presenting any specific solutions, it is instructive to examine the truncation errors of the prospective schemes. Two basic approaches are being considered: the conventional approach and Blottner's (ref. 3) approach. As was pointed out in the section on numerical analysis, the truncation errors are:

A. Blottner's Approach

$$\text{error in first derivative} = -\frac{(\Delta\eta_n - \Delta\eta_{n-1})}{2}\frac{\partial^2 u}{\partial\eta_2} \quad , \quad (53)$$

$$\text{error in second derivative} = -\frac{(\Delta\eta_n - \Delta\eta_{n-1})}{2}\frac{\partial^3 u}{\partial\eta_3} \quad , \quad (54)$$

and error in the nonlinear term $\frac{\partial}{\partial \eta}\left(\ell \frac{\partial u}{\partial \eta}\right)$

$$= -\frac{(\Delta\eta_n - \Delta\eta_{n-1})}{12}\left[\ell \frac{\partial^3 u}{\partial \eta_3} + 3 \frac{\partial^2}{\partial \eta_2}\left(\ell \frac{\partial u}{\partial \eta}\right)\right]_n . \quad (55)$$

Note that all the truncation errors are proportional to $(\Delta\eta_n - \Delta\eta_{n-1})$ where

$$(\Delta\eta_n - \Delta\eta_{n-1}) = (k - 1)\ \Delta\eta_{n-1} = (\eta_{n+1} - 2\eta_n + \eta_{n-1}) . \quad (56)$$

Consequently, Blottner's variable grid scheme is only first order accurate in the normal step size $\Delta\eta$ and will become second order accurate in $\Delta\eta$, provided

$$k \sim 1 + 0\ (\Delta\eta) . \quad (57)$$

Thus, unless k is a slowly varying function satisfying equation (57), the variable grid scheme is formally first order accurate.

However, the situation is entirely different if the variable grid scheme is interpreted in terms of a coordinate transformation of the type

$$\eta_n = \eta\ (N_n) \qquad (n = 1, 2, \ldots, n_{max}) . \quad (58)$$

Here, the nonuniform spacing otoη_{max} is mapped point by point into a uniform spacing, 0 to 1, in the N-coordinate, so that

$$\eta_{n+1} - 2\eta_n + \eta_{n-1} = \Delta N^2 \left(\frac{\partial^2 \eta}{\partial N}\right)_n . \quad (59)$$

Therefore, all the error terms are now proportional to ΔN^2 , and the scheme is formally second order accurate in the transformed N-plane or simply in terms of number of intervals in the normal direction.

This observation is confirmed by the variation of percentage error in wall shear plotted as a function of the number of intervals in the η-direction (fig. 3). From this figure, it is clear that except for the initial region, the curve is a straight line with a slope of 1/2 on a log-log scale. It means that the error is reduced by 1/4 each time the number of intervals is doubled, which is the true indicator of a second order accurate scheme.

B. Conventional Approach (Scheme 1)

$$\text{error in first derivative} = \frac{(\Delta\eta_{n-1} \cdot \Delta\eta_n)}{6} \frac{\partial^3 u}{\partial \eta_3}$$

$$= - \frac{k\ \Delta\eta_{n-1}^2}{6} \frac{\partial^3 u}{\partial \eta_3} \ ; \tag{60}$$

$$\text{error in second derivative} = - \frac{(\Delta\eta_n - \Delta\eta_{n-1})}{3} \frac{\partial^3 u}{\partial \eta_3}$$

$$= - \frac{(k - 1)}{3} \Delta\eta_{n-1} \frac{\partial^3 u}{\partial \eta_3} \ ; \tag{61}$$

$$\text{error in nonlinear term } \frac{\partial}{\partial \eta} \left(\ell \frac{\partial u}{\partial \eta} \right) = - \frac{(k - 1)}{12} \Delta\eta_{n-1}$$

$$\cdot \left[3\ \ell \frac{\partial^3 u}{\partial \eta_3} + 6 \frac{\partial^2 \ell}{\partial \eta_2} \cdot \frac{\partial u}{\partial \eta} + 6 \frac{\partial^2 u}{\partial \eta_2} \cdot \frac{\partial \ell}{\partial \eta} \right] . \tag{62}$$

Thus the first derivative is second order accurate in $\Delta\eta$, whereas the second derivative and the nonlinear terms are only first order accurate in $\Delta\eta$. This makes the difference equations slightly inconsistent and results in much higher error in the solution when compared to Blottner's approach on a one-to-one basis.

However, in terms of the N-coordinate, all the truncation errors are proportional to ΔN^2, and again this is confirmed by plotting percentage error in the solution versus the number of intervals. The curve is a straight line of slope 1/2 on a log-log scale (fig. 3), as was the case for Blottner's approach. However,

note the level of error in the two cases, e.g., with 32 points Blottner's scheme gives an error of 2.5 percent compared to a 27 percent error in the conventional scheme. Another interesting observation is that the conventional approach would not converge with 25 points, whereas with the Blottner's scheme we get an error of about 4 percent in the wall shear with 25 points.

It should be mentioned here that these error estimates are based on the exact numerical solution as the reference, the exact numerical solution being obtained by Richardson's extrapolation applied to the two most accurate numerical solutions computed here. The test problem for all the results in this section, unless mentioned otherwise, is a flat plate at $M_\infty = 2.8$, the test conditions being identical to the experimental study of Moore and Harkness (ref. 18).

C. Conventional Approach (Scheme 2)

Another series of runs was made to test the effect of inconsistency in the first derivative in the conventional approach, and it is designated here as scheme 2 of the conventional approach.

This scheme is the same as the conventional approach (scheme 1) with the exception that the first derivative expressions are replaced with

$$\frac{\partial u}{\partial \eta} = \frac{u_{n+1} - u_{n-1}}{\Delta\eta_{n-1} + \Delta\eta_n} \quad . \tag{63}$$

Consequently, the truncation errors in all the terms are proportional to $(k - 1)\ \Delta\eta_1$ where

$$(k - 1)\ \Delta\eta_1 = \Delta N^2 \left(\frac{\partial^2 \eta}{\partial N_2}\right) \quad . \tag{64}$$

The results obtained with this scheme are also plotted on figure 3. Undoubtedly, the scheme is second order accurate in the number of intervals, and results thus obtained are much closer to

the Blottner's scheme. The conventional approach conveys the important idea that all the difference expressions should always be of the same accuracy for the sake of consistency. However, there is still a noticeable difference in the results in comparison to Blottner's scheme, and this is attributed to the different treatment of nonlinear terms of type $\frac{\partial}{\partial \eta}\left(\ell \frac{\partial u}{\partial \eta}\right)$. Although the truncation errors are formally of the same order, the coefficients in the error terms are not the same, which result in the type of differences seen in figure 3.

D. Effect of Turbulence Modeling

A final test case in this study on truncation errors was aimed at assessing the influence of the turbulence model on the accuracy of the solution. The turbulence model used here has an explicit dependence on the boundary layer thickness, which is not a well-defined quantity, especially when the calculations are made with 20 to 30 mesh points; because, in such cases, we do not have a sufficient number of points in the outer part of the boundary layer to achieve an exponential decay of the profiles. Following the lead of Mellor and Herring (ref. 19), the outer eddy viscosity was assumed constant. The results obtained with this model are plotted in figure 4, along with the results of using the conventional two-layer eddy viscosity model (refs. 7 to 10). The numerical scheme used in both cases is Blottner's scheme. It is clear from figure 4 that the solution is significantly more accurate (using the same number of mesh points), with this model as opposed to the conventional eddy viscosity model where the outer viscosity goes to zero at the edge of the boundary layer. This opens up the possibilities of employing a more suitable turbulence model which does not depend on the boundary layer thickness explicitly and at the same time is physically acceptable.

Having established the overall numerical accuracy of Blottner's variable grid scheme, as employed here, a few comparisons are made with experimental data and other numerical solutions to test the present scheme.

(1) Turbulent Flat Plate

A high Reynolds number flow is chosen here, with test conditions identical to the experimental study of Moore and Harkness (ref. 18) which are as follows:

$$M_\infty = 2.8 \ ,$$

$$p_{t,\infty} = 0.997 \ \text{MN/m} \ ,$$

$$T_{t,\infty} = 311.1°\text{k} \ ,$$

and

$$T_w/T_{t,\infty} = 0.95 \ .$$

Since transition location was not reported in reference 18, the only comparisons shown here are for the fully turbulent flow. The numerical results presented in figure 5 compare well with the experimental data, and were obtained with $n_{max} = 41$ and $k = 1.275$.

(2) Laminar, Transitional, and Turbulent Flow on Sharp Cone

The case under consideration is a 10° sharp cone for which experimental data was obtained by Stainbeck (ref. 20) at the NASA Langley Research Center. The test conditions are as follows:

$$M_\infty = 8 \ ,$$

$$p_{t,\infty} = 17.38 \ \text{MN/m}^2 \ ,$$

$$T_{t,\infty} = 759.4° \ \text{k} \ ,$$

and

$$T_w/T_{t,\infty} = 0.42 \ .$$

The location and extent of transition were taken from the experimental data, and the resulting solutions are shown in figure 6. Present results compare reasonably well with the experimental data except near the end of the transition where the present calculations fail to reach the measured overshoot in the heating rate. The discrepancy arises largely because of the choice of the recovery factor in the transition region. After the transition, present results compare well with the turbulent data. It should be noted that these numerical results were performed with 41 points in the boundary layer.

(3) Laminar Flow with Mass Injection

Marvin and Akin (ref. 21) obtained data over a range of injection rates for a sharply tipped 5° cone. The cone was solid for $X < 9.53$ cm, and the remainder of the cone was porous. The test conditions are as follows:

$$M_\infty = 7.4 \ ,$$

$$p_{t,\infty} = 4.137 \ \text{MN/m}^2 \ ,$$

$$T_{t,\infty} = 833.3° \ \text{k} \ ,$$

and

$$T_w/T_{t,\infty} = 0.38 \ .$$

The air injection parameter $\tilde{F}$, defined as

$$\tilde{F} = \frac{(\rho v)_w}{(\rho u)_e} \ , \tag{65}$$

ranged from a minimum of zero (no injection) to a maximum value of 1.3903×10^{-3} .

The heating rate normalized by the heating rate at the wall at $x = 9.53$ cm is presented in figure 7A along with the

experimental data of Marvin and Akin (ref. 21) for 4 different values of $\tilde{F}$. It should be noted that mass distribution was not uniform in the experimental study (see ref. 6), whereas the computations reported here were carried with an average value of mass injection. Considering the uncertainties in the experimental mass distribution, the results obtained here compare well with the experimental data over the large range of mass injection. The velocity profiles at $X/L = 1.574$ are also shown for these cases in figure 7B, and it is apparent that for $F = 1.3903 \times 10^{-3}$, i.e., for the maximum mass injection base, the flow is approaching separation.

(4) Laminar Blunt Body Flow

The case chosen here is a hemispherical nose, the test conditions being:

$$M_\infty = 10.4 ,$$

$$p_{t,\infty} = 10.77 \text{ MN/m}^2 ,$$

$$T_{t,\infty} = 1222^\circ \text{ k} ,$$

and

$$T_w/T_{t,\infty} = 0.25 .$$

Numerical solutions for this case have been obtained by Marvin and Sheaffer (ref. 22). The heating rate and shear stress at the wall, normlized with their respective maximum values, are presented in figures 8A and 8B along with the results of reference 22. The modified Newtonian inviscid pressure distribution was used in the present calculations. Since Marvin and Sheaffer (ref. 22) have not given the details of the inviscid pressure used, results are presented only up to the point where the pressure gradient is favorable. Comparison between the two approaches is

excellent keeping in view the fact that the source of the inviscid pressure may not be the same in both approaches. The present calculations were made with 31 points in the boundary layer.

CONCLUSIONS AND RECOMMENDATIONS

An extremely efficient numerical scheme has been identified. The scheme utilizes highly nonuniform mesh width distribution in the boundary layer and achieves reasonably accurate solutions for turbulent boundary layers with 25 to 30 nodes. The scheme is shown to give good results for a variety of problems.

Further research will be directed in utilizing this approach for the more challenging, three-dimensional turbulent boundary layer calculations.

Table 1. Effect of iteration of wall shear.

$CF_e \times 10^2$

S \ No. of Iterations	0	1	2	15
1.0	.13753	.13736	.13752	.13765
2.0	.12187	.12416	.12441	.12450
3.0	.11443	.11635	.11661	.11668
4.0	.11133	.11288	.11306	.11310
5.0	.10874	.10936	.10948	.10951
6.0	.10581	.10614	.10623	.10626
7.0	.10329	.10374	.10383	.10385
8.0	.10167	.10234	.10242	.10244
9.0	.10066	.10128	.10136	.10137
10.0	.09976	.10024	.10030	.10031

Table 2. Geometric progression constant employed by various investigators.

Author(s)	Reference Number	k	No. of Intervals
Smith and Cebeci	7	1.02	157
Anderson and Lewis	12	1.09	100
Verma	13	1.07	100
Adams	14	1.063	85
Dwyer et al.	15	1.021	350
Shang et al.	16	1.04-1.12	294-112
Bushnell and Beckwith	17	1.02	230

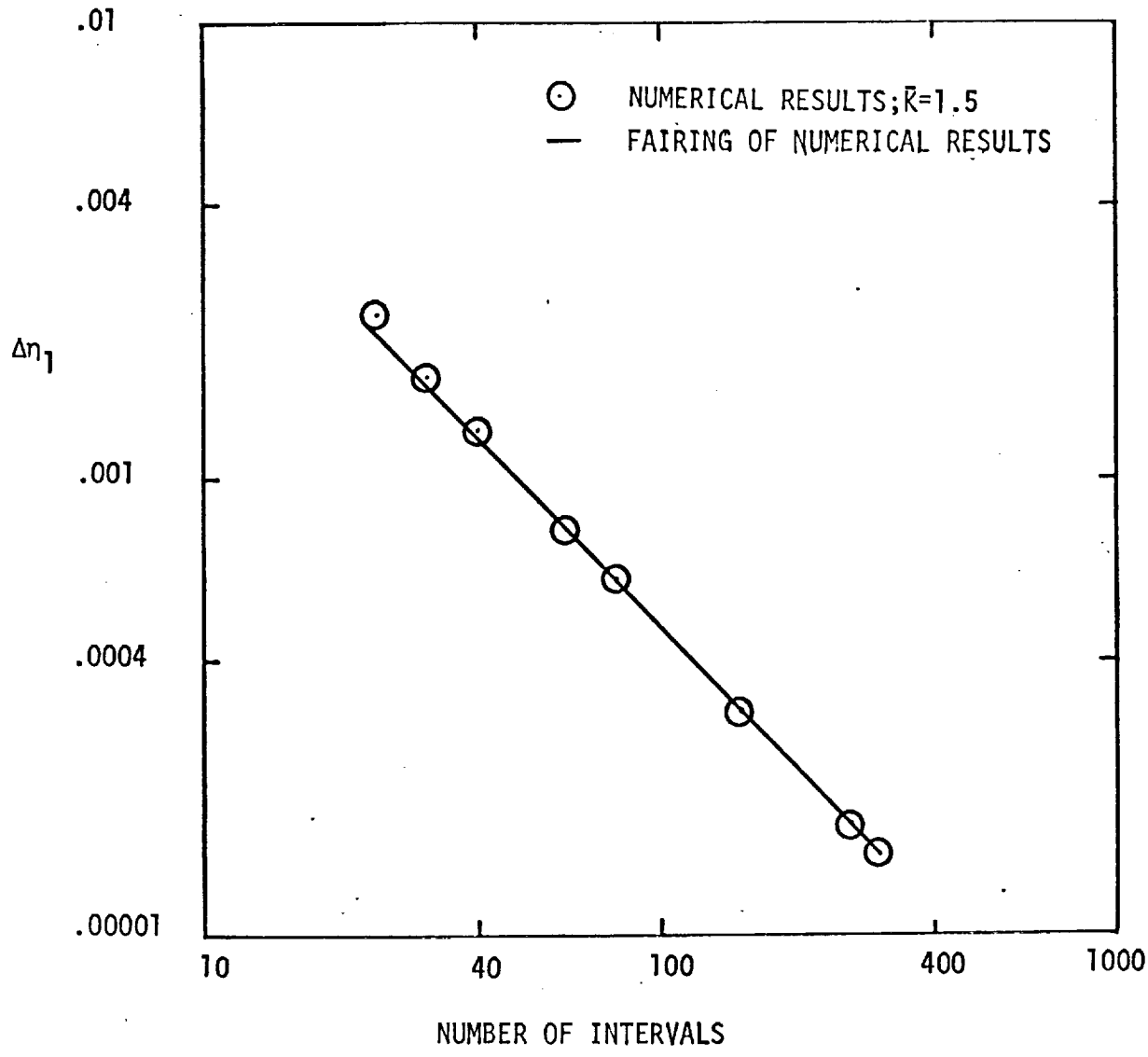

Figure 1. Effect of No. of intervals on step size at the wall.

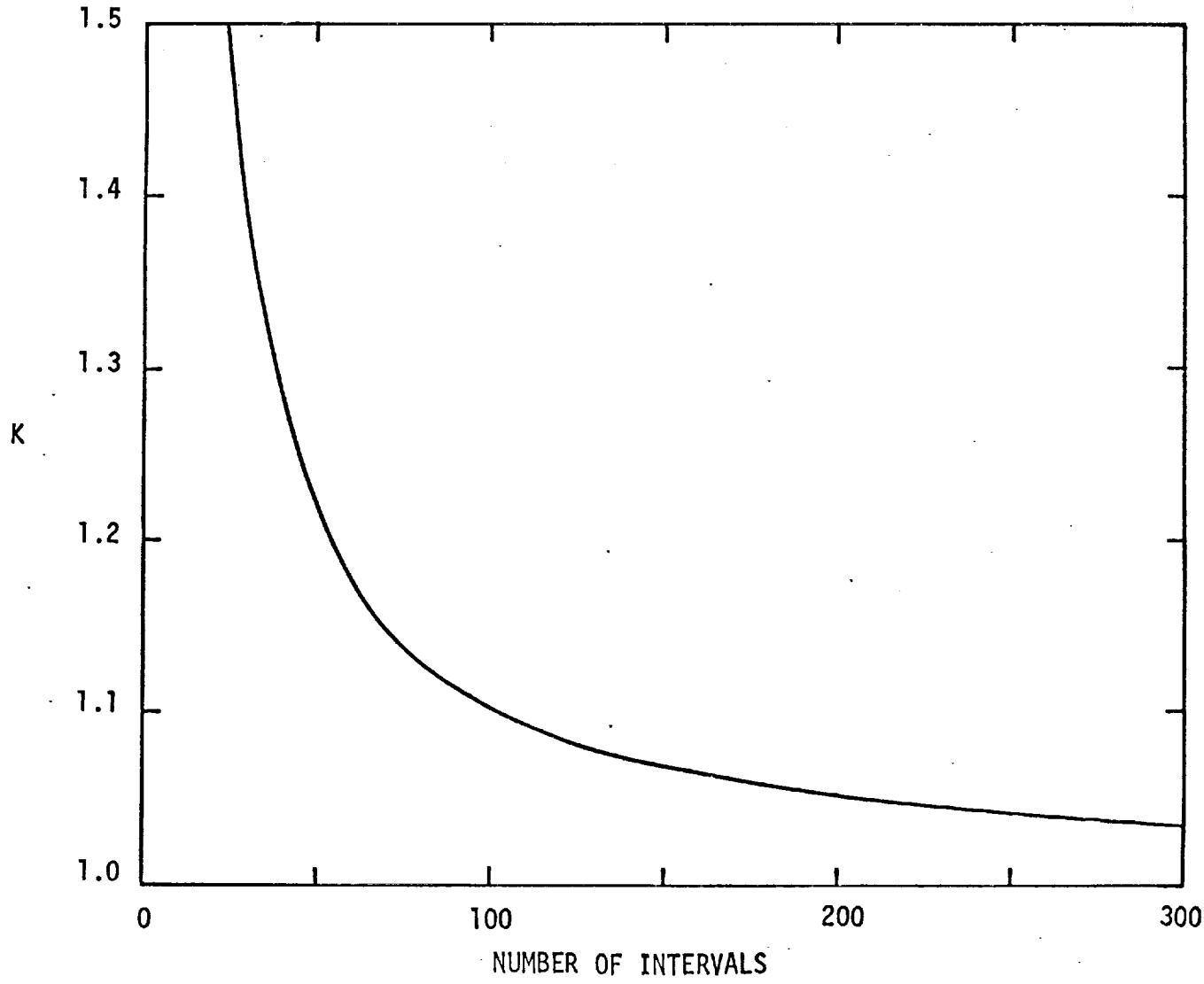

Figure 2. Geometric progression constant for $\overline{K} = 1.5$.

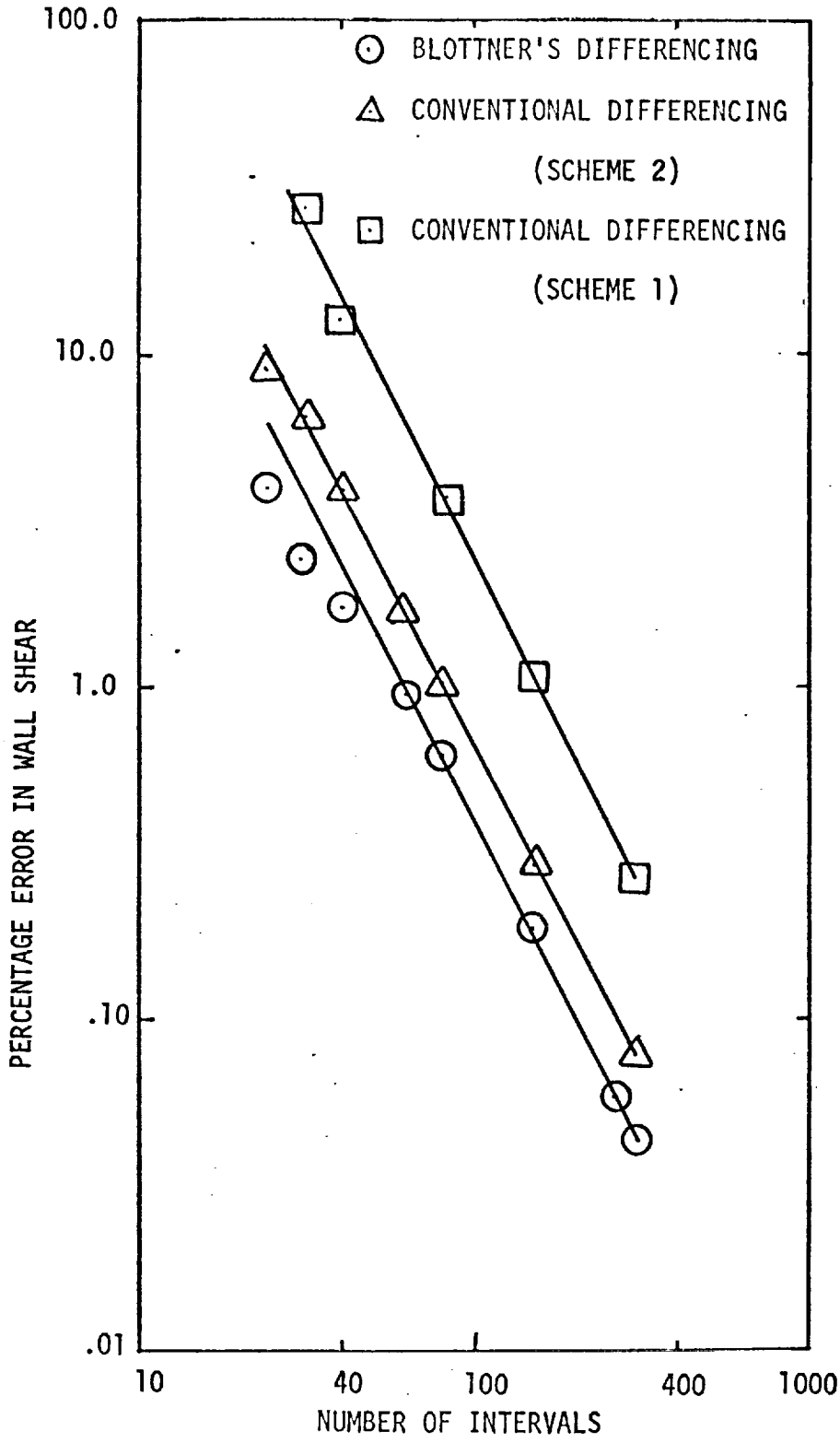

Figure 3. Comparison of difference schemes.

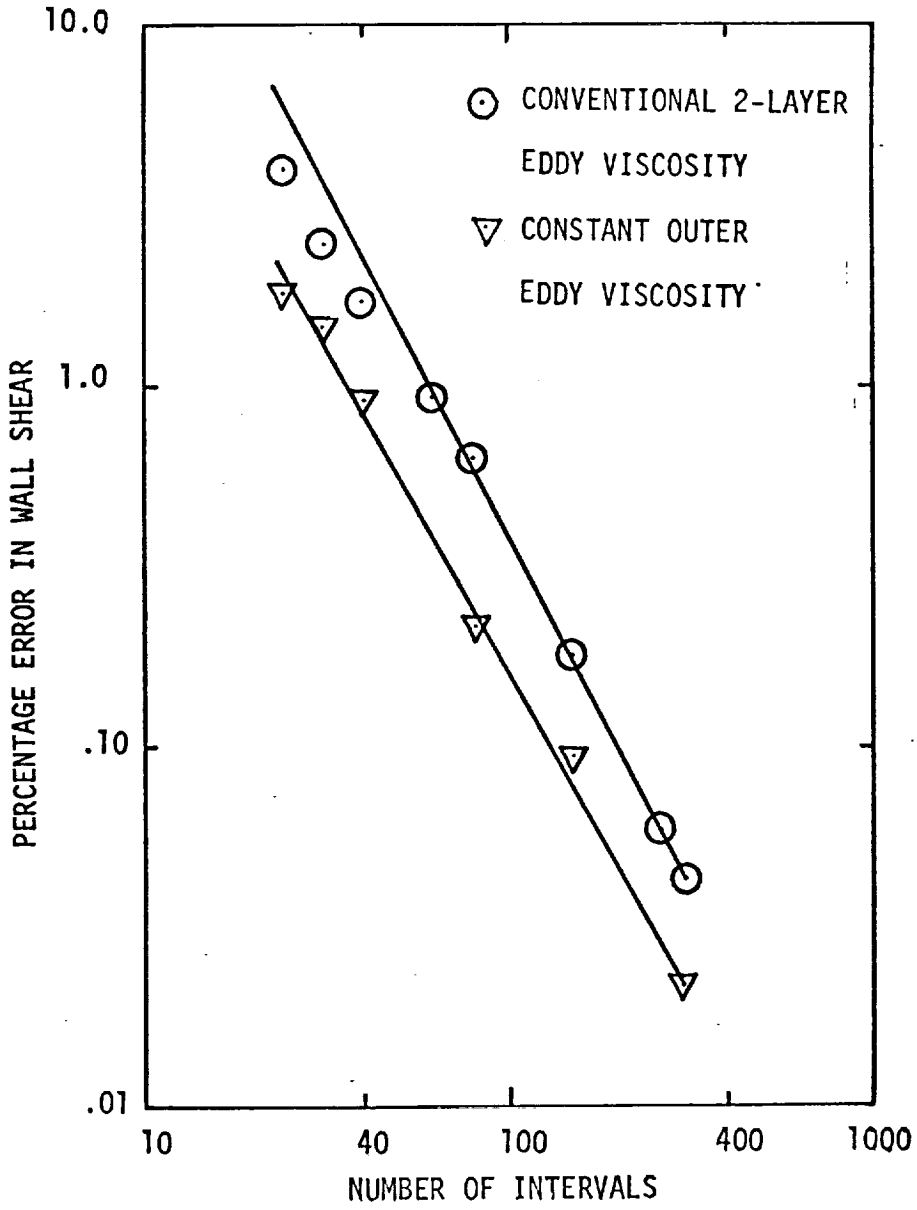

Figure 4. Effect of turbulence model.

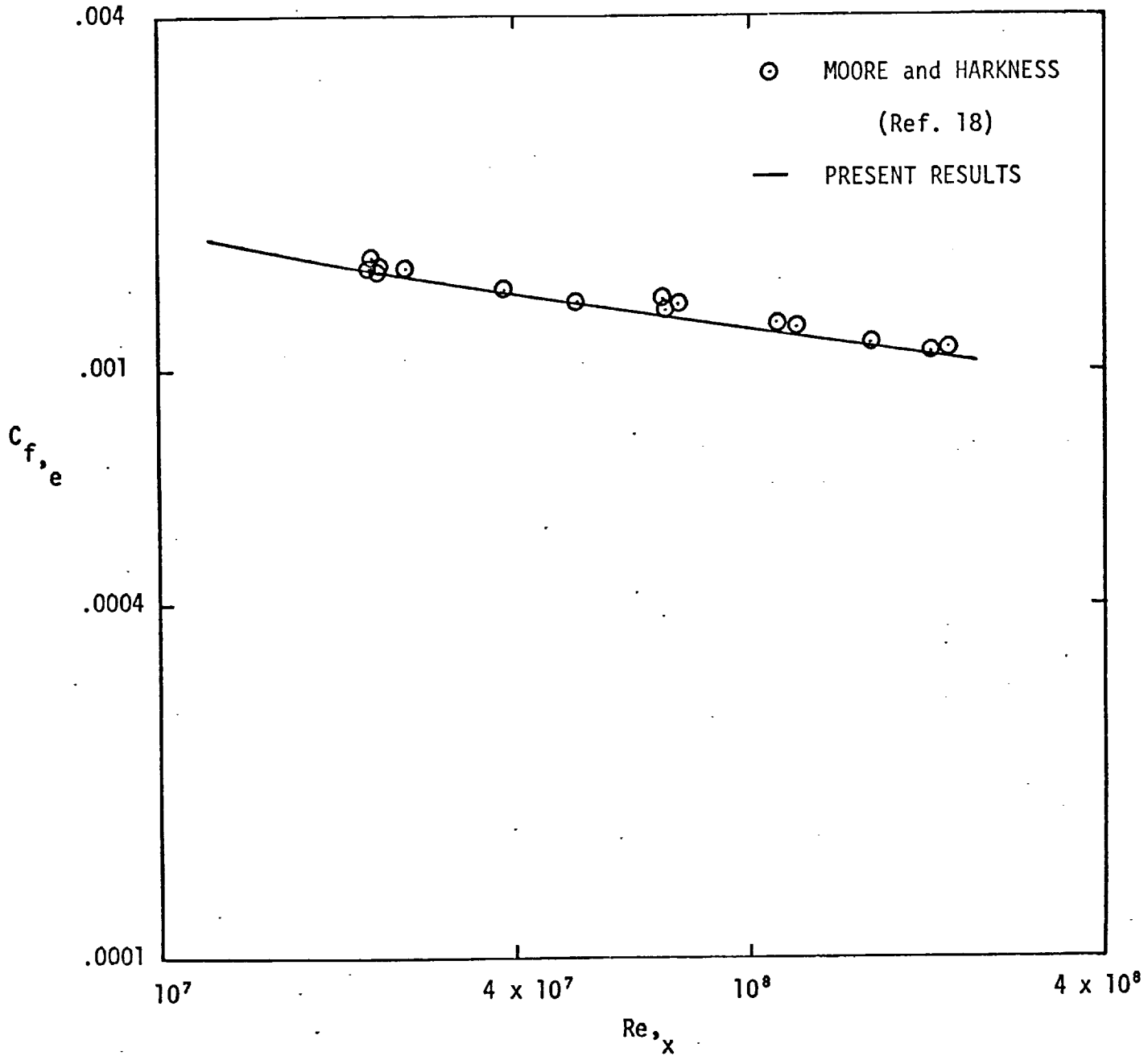

Figure 5. Turbulent flow over flat plate.

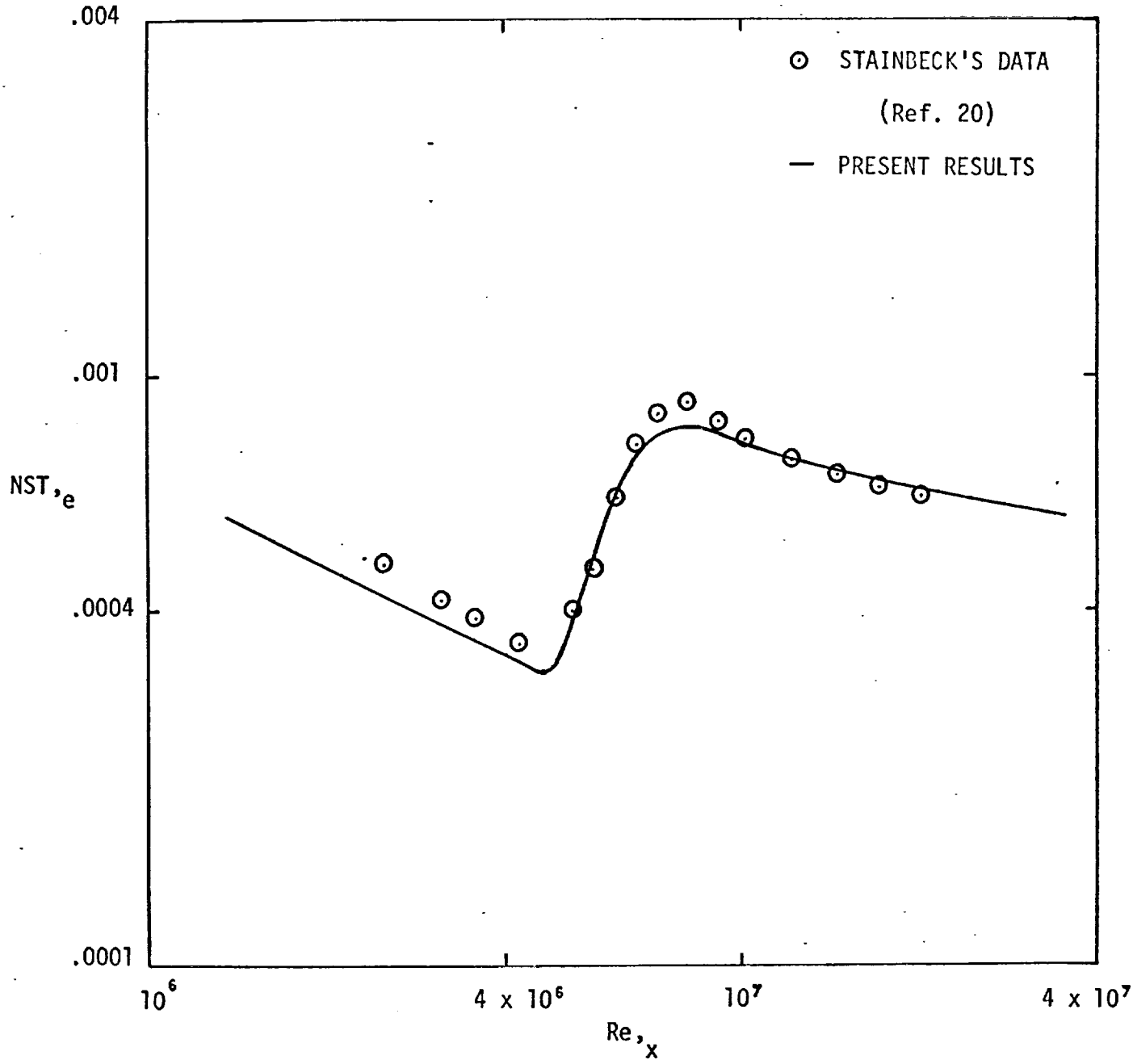

Figure 6. Turbulent flow over sharp cone.

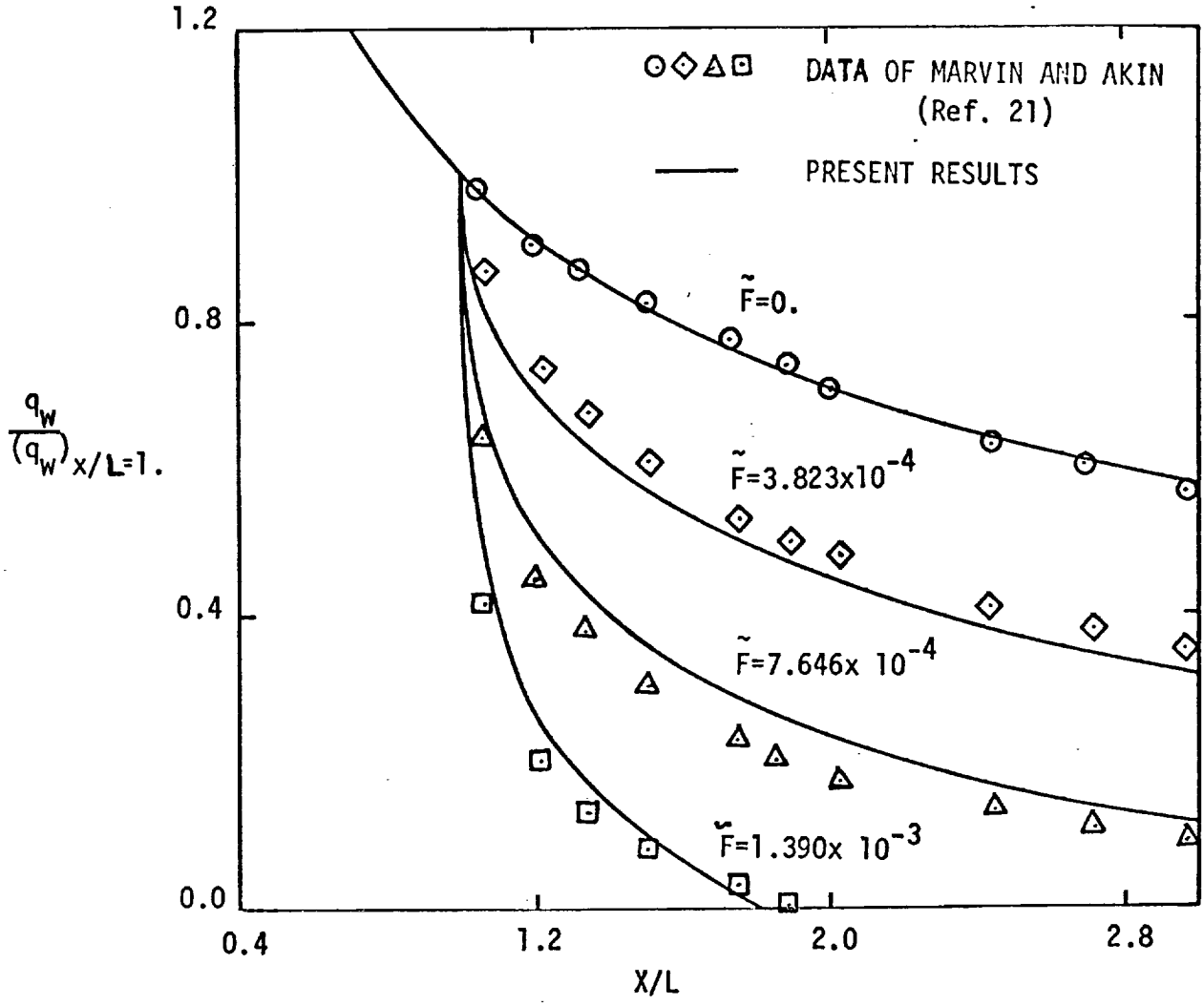

Figure 7A. Heat transfer for sharp laminar cone with mass injection.

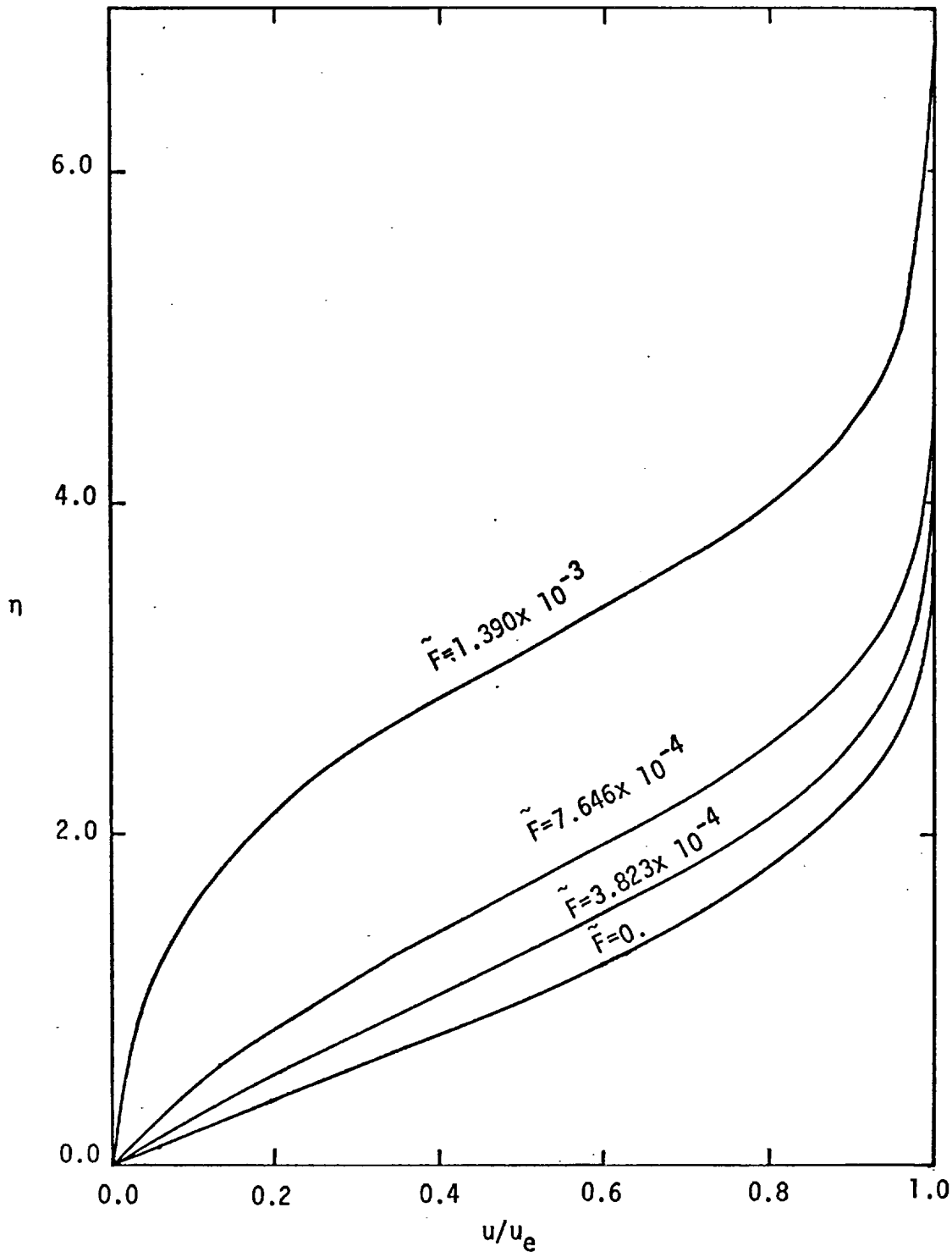

Figure 7B. Velocity profile for sharp laminar cone with mass injection; X/L = 1.574.

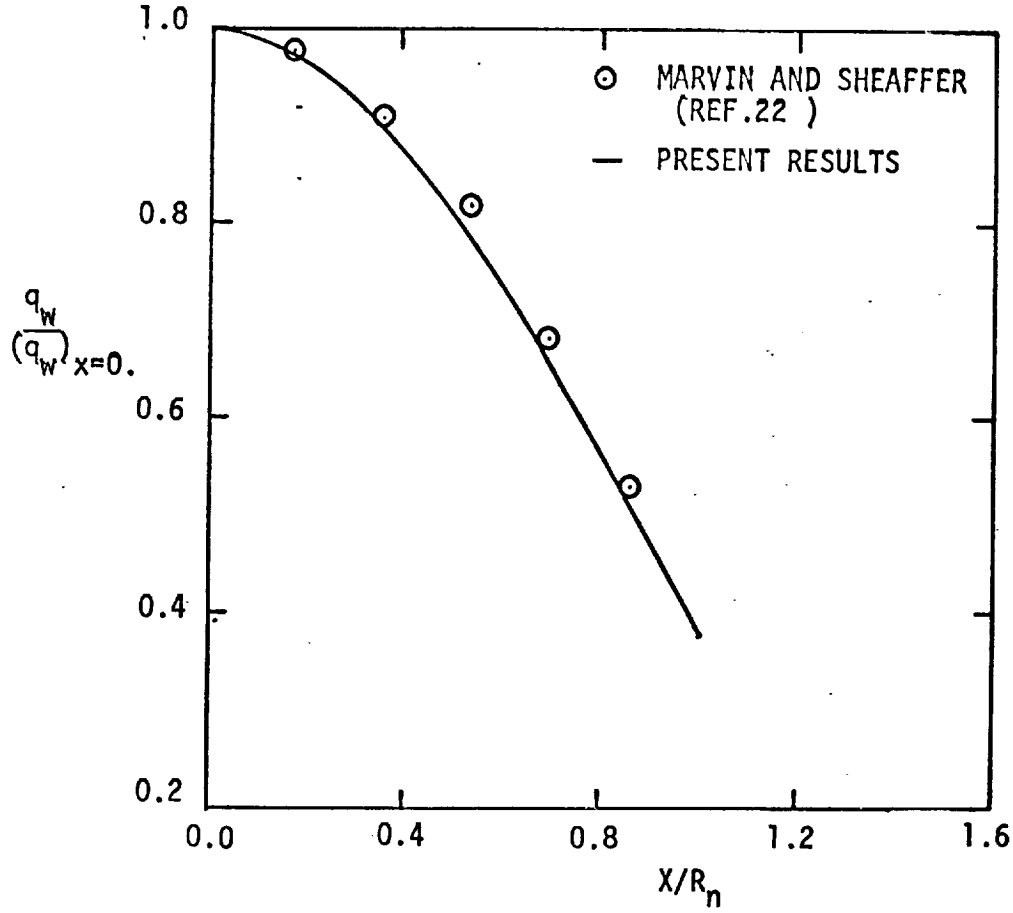

Figure 8A. Heat transfer for spherical cap.

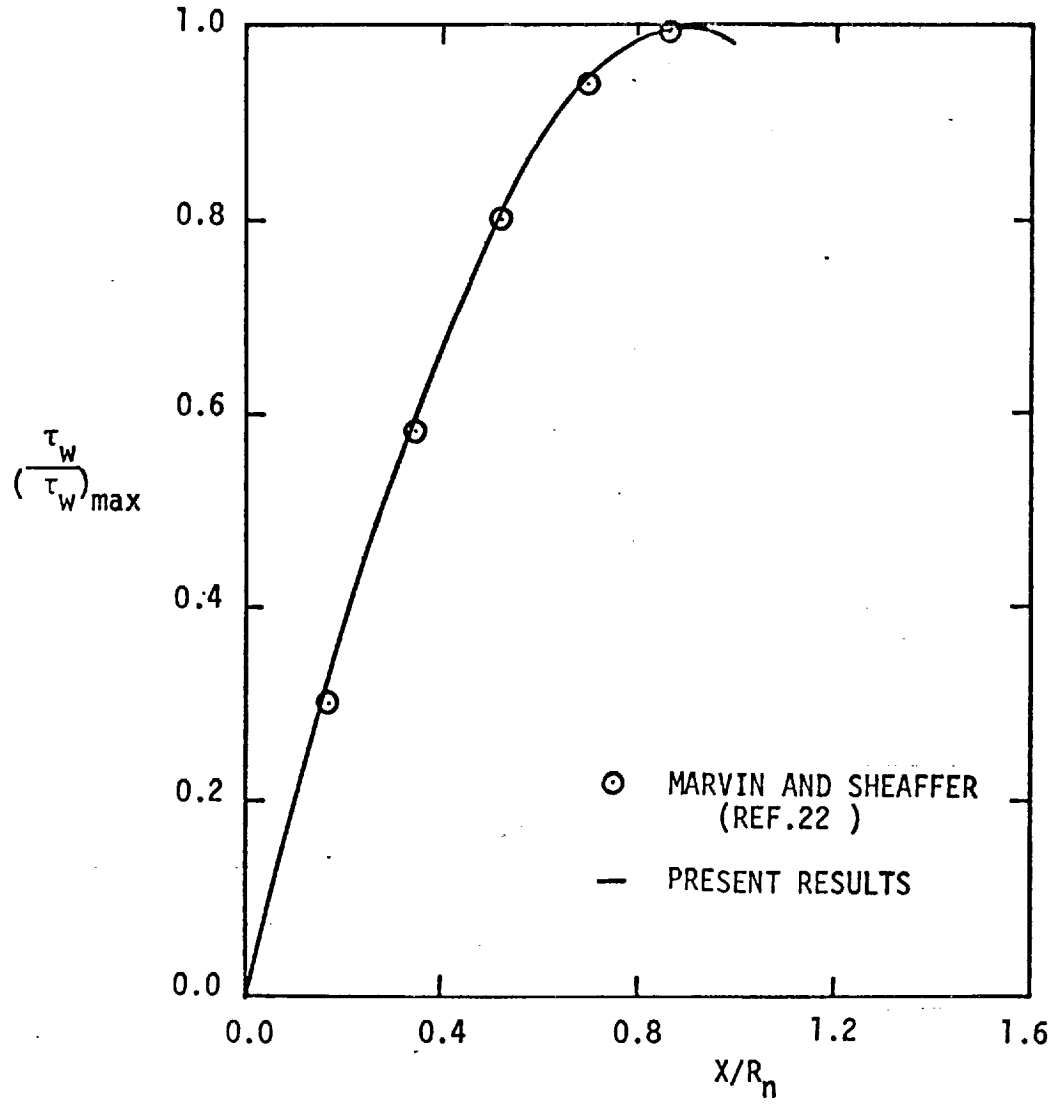

Figure 8B. Wall shear for spherical cap.

REFERENCES

1. Kline, S. J., M. V. Morkovin, G. Sovran, and D. S. Cockrell. Computation of Turbulent Boundary Layers. AFOSR-IFP, Stanford Conferences, Vols. I and II. Stanford University Press, Stanford, California, 1968.

2. Keller, H. B. and T. Cebeci. Accurate Numerical Methods for Boundary Layer Flows II: Two-dimensional Turbulent Flows. AIAA Journal, Vol. 10 (1972), pp. 1193-1199.

3. Blottner, F. G. Variable Grid scheme Applied to Turbulent Boundary Layers. Computer Methods in Applied Mechanics and Engineering, Vol. 4, 1974, pp. 179-194.

4. Schlichting, H. Boundary Layer Theory, 6th ed. McGraw-Hill Book Company, New York, 1968.

5. VanDriest, E. R. Turbulent Boundary Layer in Compressible Fluids. Journal of Aeronautical Sciences, Vol. 18, No. 3, March 1951, pp. 145-160, 216.

6. Harris, Julius E. Numerical Solution of the Equations for Compressible Laminar, Transitional, and Turbulent Boundary Layers and Comparisons with Experimental Data. NASA TR R-368, 1971.

7. Smith, A. M. O. and T. Cebeci. Numerical Solution of the Turbulent Boundary Layer Equations. Report No. DAC 33735. Douglas Aircraft Company, May 29, 1967.

8. Harris, J. E. Numerical Solution of the Compressible Laminar, Transitional, and Turbulent Boundary Layer Equations with Comparisons to Experimental Data. Ph.D. thesis, Virginia Polytech. Inst., May 1970.

9. Cebeci, T. and A. M. O. Smith. A Finite-Difference Method for Calculating Compressible Laminar and Turbulent Boundary Layers. Journal of Basic Engineering, September 1970, pp. 523-535.

10. Price, J. M. and J. E. Harris. Computer Program for Solving Compressible Nonsimilar Boundary Layer Equations for Laminar, Transitional or Turbulent Flows of a Perfect Gas. NASA TM X-2458, April 1972.

11. Carnahan, B., M. A. Luther, and J. O. Wilkies. Applied Numerical Methods. John Wiley & Sons, Inc., New York, 1969.

12. Anderson, E. C. and C. H. Lewis. Laminar or Turbulent Boundary Layer Flows of Perfect Gas or Reacting Gas Mixtures in Chemical Equilibrium. NASA CR-1893, October 1971.

13. Verma, V. K. A Method of Calculation for Two-dimensional and Axisymmetric Boundary Layers. University of Cambridge report, CVED/A-Aero/TR3, 1971.

14. Adams, Jr., J. C. Eddy-Viscosity Intermittency Factor Approach to Numerical Calculation of Transitional Heating on Sharp Cones in Hypersonic Flows. AEDC-TR-70-210, November 1970.

15. Dwyer, H. A., E. D. Doss, and A. L. Goldman. A Computer Program for the Calculation of Laminar and Turbulent Boundary Layer Flows. NASA CR-114366, 1972.

16. Shang, J. S. and W. L. Hankey. Numerical Analysis of Eddy Viscosity Models in Supersonic Turbulent Boundary Layers. AIAA paper no. 73-164, presented at the AIAA 11th Aerospace Sciences Meeting held at Washington, D.C., January 10-12, 1973.

17. Bushnell, Dennis M. and Ivan E. Beckwith. Calculation of Nonequilibrium Hypersonic Turbulent Boundary Layers and Comparisons with Experimental Data. AIAA Journal, Vol. 8, No. 8, August 1970, pp. 1462-1469.

18. Moore, D. R. and J. Harkness. Experimental Investigation of the Compressible Turbulent Boundary Layer at Very High Reynolds Numbers, M = 2.8. Rep. No. 0-71000/4R-9. LTV Research Center, April 1964.

19. Herring, H. J. and G. L. Mellor. Computer Program for Calculating Laminar and Turbulent Boundary Layer Development in Compressible Flow. NASA CR-2068, June 1972.

20. Stainbeck, P. C. Use of Rouse's Stability Parameter in Determining the Critical Layer Height of a Laminar Boundary Layer. AIAA Journal, Vol. 8, No. 1, January 1970, pp. 173-175.

21. Marvin, J. G. and C. M. Akin. Combined Effects of Mass Addition and Nose Bluntness of Boundary Layer Transition. AIAA paper no. 69-706, June 1969.

22. Marvin, J. G. and Y. S. Sheaffer. A Method for Solving the Nonsimilar Laminar Boundary Layer Equations Including Foreign Gas Injection. NASA TND-5516, 1969.